12.3 Toy model simulations of surface vorticity generation in downdrafts

Matthew D. Parker[1]
Johannes M. L. Dahl[1,2]

[1]Department of Marine, Earth, and Atmospheric Science, North Carolina State University
[2]*Current affiliation:* Department of Geosciences, Texas Tech University

1. Introduction

Full-physics simulations of supercells suggest that surface vertical vorticity (a pre-condition for tornadogenesis) is rather unsteady and tied to parcels emanating from downdrafts adjacent to the main updraft (Davies-Jones and Brooks 1993). The configuration of the resulting surface vertical vorticity maxima, including their orientation, intensity, and storm-relative motion, results from some combination of baroclinic and barotropic processes in the downdraft (e.g. Straka et al 2007, Dahl et al 2013). Operationally, it is also known that parameters based upon the low-level wind profile are somewhat skillful in identifying significant tornado days (Markowski et al. 2003); the physical explanation for this skill is not yet totally clear. The difficulty with hypothesis tests using full supercell simulations is that, when the environment is varied, many storm-scale features change.

We are therefore undertaking idealized sensitivity tests in which simple downdrafts are introduced with various configurations into environments with different magnitudes and orientations of low-level shear. Such work bears some resemblance to previous idealized studies (Walko 1993, Markowski and Richardson 2013), but here we undertake a broad matrix of sensitivity tests that specifically focus on the resulting structures of simulated surface vertical vorticity maxima. The long range goal of this study is to establish the role of the low-level wind profile in downdraft generation of vertical vorticity, and to establish the conditions under which baroclinic production or barotropic rearrangement of vertical vorticity is likely to predominate.

2. Methods

Our basic method in most ways mirrors the model configuration for the full-physics supercell simulations of Dahl et al (2013). We perform 3D simulations using CM1 version 16 (Bryan and Fritsch 2002) with horizontal grid spacing of 250 m and vertical grid spacing that is stretched from 100 m at the surface to 250 m aloft. The model is run dry (no condensation processes are present), and the environmental sounding has constant potential temperature. All other settings are identical to those used by Dahl et al (2013), and are available from the authors by request.

We refer to these simple experiments as "toy model" simulations because we artificially trigger downdrafts by applying four different kinds of forcing, as summarized in Table 1. In each case, the forcing is Gaussian in shape (with peak amplitude as given in Table 1), having a horizontal and vertical radius of 1.4 km. The peak amplitudes are set so as to produce downdrafts with comparable vertical velocities among all treatments. The bubble triggers represent initial perturbations that then freely evolve with the flow; the tendency triggers are fixed in location, with air flowing through the forcing zone over time. There is no forcing for updraft applied in these simulations.

The environment has no initial vertical vorticity, so all vertical vorticity that emerges must be produced by the artificial downdrafts that we instigate. Based upon previous studies (e.g. Davies-Jones and Brooks 1993) and our ongoing work (Dahl et al 2013), we are interested in understanding the specific role of the crosswise horizontal vorticity component upon barotropic production of vertical vorticity. Therefore, in the present experiments we vary this crosswise component by systematically changing the angle of the wind profile's horizontal vorticity vector with respect to the wind vector through the 0-3 km layer (see hodographs in Figure 1). For example, in the "25L" experiment, the horizontal vorticity vector is oriented 25° to the left of the environmental wind vector at every level. The two simple limiting cases are the purely streamwise case ("0/stream") and the purely crosswise case (90/cross). An un-sheared profile (using the mean wind from the 0/stream case) is also tested for comparison. Every profile (except for the un-sheared case) has an identical surface wind vector and an identical magnitude of environmental horizontal vorticity ($0.005\ s^{-1}$). Each forcing-hodograph combination is simulated using both free-slip and no-slip bottom boundary conditions for comparison.

Corresponding author's address: Matthew D. Parker, Campus Box 8208, NC State University, Raleigh, NC, 27695-8208.

3. Preliminary Results

As shown in Figure 2 for the simple case of a cold bubble in streamwise horizontal vorticity, the response of the flow to the instigated downdraft involves the generation of vertical vorticity. Much as depicted by Straka et al (2007), the resultant vortex lines show evidence of both barotropic rearrangement of vorticity (these are the valleys of downward vortex line displacement, following Helmholtz's theorem) as well as baroclinic generation and subsequent tilting of additional horizontal vorticity (these are the rings and arches of vortex lines attached to zones of baroclinity). For this case, it is seen (Figure 2) that the mid-level maximum in vertical vorticity (red isosurface) is primarily associated with the "barotropic valleys" in vortex lines; however, the surface vertical vorticity beneath this is rather small. This is in part because the vertical vorticity is weakened by horizontal divergence at the base of the downdraft, but also because the initially streamwise vorticity becomes parallel to the ground at the foot of the downdraft (as explained by Davies-Jones and Brooks 1993). In contrast, the maximum in surface vertical vorticity, as indicated in Figure 2, is primarily associated with a "baroclinic arch" along the western edge of the outflow. These combined effects of barotropic and baroclinic production of vertical vorticity are seen occur in all of the simulations to some degree (with the exception of the un-sheared runs in which there is no initial horizontal vorticity), and should be regarded as the inevitable results of downdraft production within vertical wind shear.

Within this context, useful differences exist among the 56 simulations outlined in Section 2. A time history of surface vertical vorticity (Figure 3) supports several key themes. First, the runs with persistent tendencies (the bottom row of Figure 3) almost universally produce larger surface vertical vorticity than the runs with initial bubbles (the top row of Figure 3). This is likely partly due to the enhanced gust front convergence within runs with continual downdraft forcing. However, it also appears that ongoing "flow through" a downdraft is beneficial because it continually introduces parcels from different initial altitudes to the surface, which (from Helmholtz's theorem) implies considerable tilting of the initial distribution of environmental horizontal vorticity. Secondly, it appears that the larger surface vertical vorticity values generally occur in the runs with cooling (not just direct forcing of w). This may again be partly related to the enhancement of gust front convergence. But, localized cooling also implies that buoyancy gradients (and hence, continued baroclinic generation of horizontal vorticity) may persist after parcels have departed from the downdraft (since, as denoted in Table 1, parcels only carry negative buoyancy away from the downdraft in the cooling runs). A final general result is that surface drag has little influence on the surface vertical vorticity beyond slightly weakening the peak values in most runs. This influence of drag is therefore not discussed further.

The most striking result shown in Figure 3 is that the 25L and 15L runs with cooling tendency produce much larger surface vertical vorticity than any other runs in the experiment, and far exceed the corresponding 0/stream, 15R, and 25R cooling tendency simulations. This strong sensitivity to the environmental wind profile is quite relevant to the long range goals of our study. Cursory examination of snapshots from the 25L and 25R runs (Figure 4) shows similar downdraft structures (gray isosurfaces), with a mid-level maximum in vertical vorticity to the west of the downdraft in both cases (red isosurfaces). Both runs show evidence of barotropic downward displacement of vortex lines as well as baroclinic vortex line rings extending around the perimeter of their surface cold pools. The primary difference between the runs (Figure 4) is that the (primarily baroclinically-generated) surface vertical vorticity maximum occurs on the upwind (east-southeast) side of the downdraft in the 25L run, versus the downwind (west-northwest) side of the downdraft in the 25R run. Thus, in the 25L run, the high vorticity parcels exit the downdraft and do not spread very far away, remaining in a regime of strong convergence (where their vertical vorticity amplifies). In the 25R run, the high vorticity parcels exit the downdraft and move rapidly away in the downstream direction, not profiting substantially from sustained convergence. The difference in the fates of the downdraft parcels appears to be directly linked to the differences in subsequent surface vertical vorticity.

Air parcel trajectories in the 25L run (Figure 5) reveal a familiar structure that is common to many full-physics simulations of supercells. Parcels from the lowest ~1 km AGL descend along the edge of the downdraft. This is a zone with a large radial gradient in buoyancy, and thus significant baroclinic generation of horizontal vorticity. These trajectories curve cyclonically during and after descent, a "river bend" maneuver that has been shown to facilitate the crosswise to streamwise conversion of horizontal vorticity (e.g. Dahl et al 2013, Markowski and Richardson 2013). Finally, these parcels emerge from the downdraft within internal surges or rivers of large surface vertical vorticity. Because the internal surges within the 25L (and also 15L) runs are preferentially into a zone of strong

convergence, the vertical vorticity increases rapidly there within a few minutes. Although our present toy model simulations do not include any imposed forcing for ascent, it is intriguing to note that in nature this convergent zone southeast of the main downdraft is generally where the parent storm's updraft (and attendant dynamic lifting) would be found. Therefore, among all wind profiles tested, the 25L profile produces a footprint of surface vertical vorticity that seems to be most optimized for producing a tornado.

4. Conclusions

Our initial experiments support the following tentative conclusions. Realistic surface vortices are produced in this toy model, and the vortices are fundamentally downdraft/outflow phenomena. Barotropic rearrangement and baroclinic production of vertical vorticity co-exist in these simulations; surface vertical vorticity often is small beneath the zone of barotropic rearrangement, whereas surface vertical vorticity associated with baroclinic production moves away rapidly in many conditions. However, it appears that the wind profile (particularly the orientation of the vertical wind shear) may play an active role within the downdraft, in part by directly influencing barotropic downdraft production of vertical vorticity, and in part by determining the directions of outflow trajectories (and thus controlling the residence times of parcels within convergent flow).

In special cases, flow through the downdraft creates a steady surface vertical vorticity maximum that is anchored immediately adjacent to the downdraft. Such a condition would seem to be favorable for tornado genesis and maintenance. In these cases, the parcels flowing into the surface vertical vorticity maximum seem to skirt the edge of the downdraft and exhibit strongly curved trajectories as they contribute to internal surges (or "rivers") or surface vertical vorticity, just as in full-physics supercell simulations.

Although our maps of vortex lines show the important behaviors qualitatively, in our ongoing work we are studying the governing dynamics more quantitatively in order to understand the substantial enhancement of surface vertical vorticity in the 25L and 15L runs. We are also performing similar experiments with varying magnitudes of vertical shear, and using in situ wind profiles extracted from the downdraft region within full-physics supercell simulations.

Acknowledgments

This work is supported by the National Science Foundation under grants ATM-0758509 and AGS-1156123. The authors thank George Bryan for his tireless support of the CM1 modeling framework, as well as beneficial discussions with Paul Markowski, Lou Wicker, and the members of the NCSU Convective Storms Group.

References

Bryan, G. H., and J. M. Fritsch, 2002: A benchmark simulation for moist non-hydrostatic numerical models. *Mon. Wea. Rev*., **130**, 2917–2928.

Dahl, J. M. L., M. D. Parker, and L. J. Wicker, 2013: The roles of ambient and storm-generated vorticity in the development of near-ground rotation within a simulated supercell. *J. Atmos. Sci.,* submitted.

Davies-Jones, R. P. and H. E. Brooks, 1993: Mesocyclogenesis from a theoretical perspective. *The Tornado: Its Structure, Dynamics, Prediction, and Hazards*, Geophys. Monogr., No. 79, Amer. Geophys. Union, 105–114.

Markowski, P., C. Hannon, J. Frame, E. Lancaster, A. Pietrycha, R. Edwards, and R. L. Thompson, 2003: Characteristics of vertical wind profiles near supercells obtained from the Rapid Update Cycle. *Wea. Forecasting*, **18**, 1262–1272.

Markowski, P. M., and Y. P. Richardson, 2013: The influence of environmental low-level shear and cold pools on tornadogenesis: Insights from idealized simulations. *J. Atmos. Sci.*, in press.

Straka, J., E. Rasmussen, R. Davies-Jones, and P. Markowski, 2007: An observational and idealized numerical examination of low-level counter-rotating vortices in the rear flank of supercells. *E-Journal of Severe Storms Meteorology*, North America, **2**, No 8.

Walko, R. L., 1993: Tornado spin-up beneath a convective cell: Required basic structure of the near-field boundary layer winds. *The Tornado: Its Structure, Dynamics, Prediction, and Hazards*, Amer. Geophys. Union, 89-95.

treatment name	forcing magnitude	continued flow through downdraft?	do parcels depart with negative buoyancy?
downdraft bubble	-20 m s^{-1}	no	no
cold bubble	-10 K	no	yes
downdraft tendency	-0.3 m s^{-1}	yes	no
cooling tendency	-0.05 K s^{-1}	yes	yes

Table 1: Fundamental parameters describing the downdraft forcing for four types of simulations. Additional details are reported in the text.

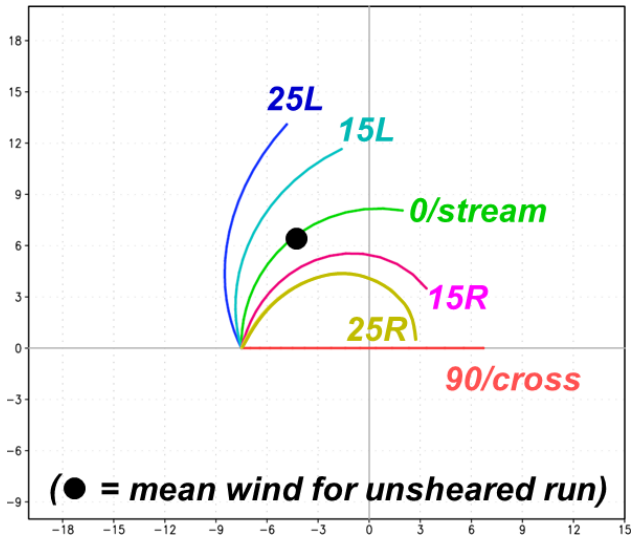

Figure 1: Hodograph diagram for the wind profiles used in this experiment. The axis labels/velocities are in m s^{-1}.

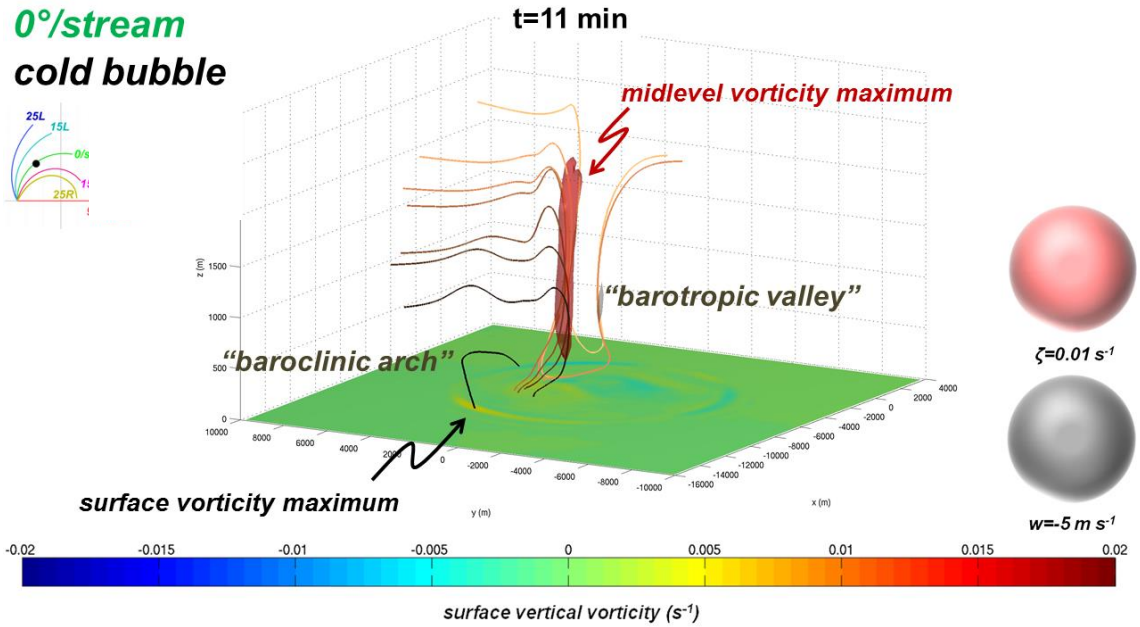

Figure 2: Three-dimensional projection of vortex lines, surface vertical vorticity (shaded as shown), and isosurfaces of vertical vorticity (red) and vertical velocity (gray) for the simulation using the initial 0/streamwise hodograph with an initial cold bubble trigger. Vortex lines are drawn through the largest vertical vorticity value at every other vertical model level.

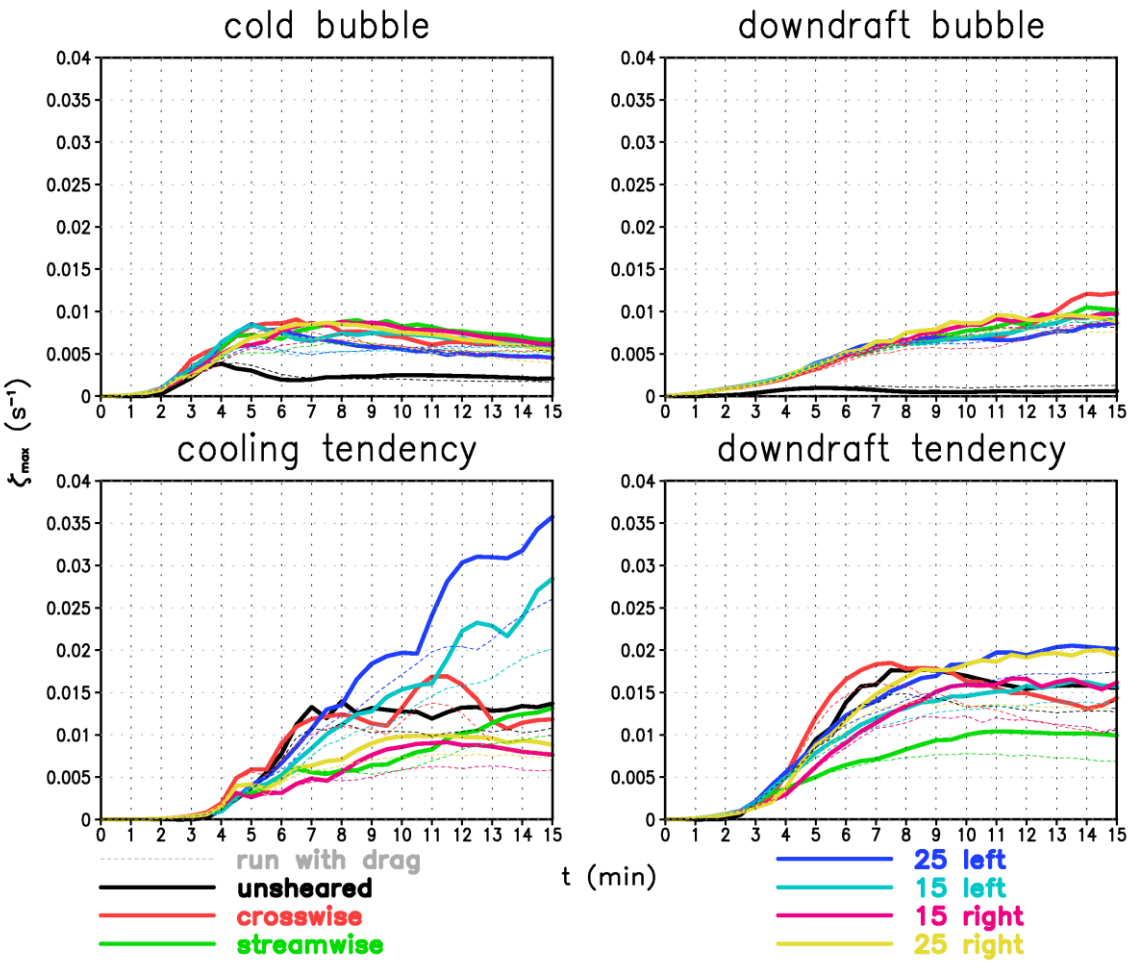

Figure 3: Time history of vertical vorticity for 56 simulations (using 7 initial hodographs, 4 downdraft forcing types, all run both with and without surface drag). The four forcing types are shown in separate panels, with the 7 unique hodographs coded by color as shown. Runs without drag are plotted with thick solid lines, runs with drag are plotted with thin dashed lines.

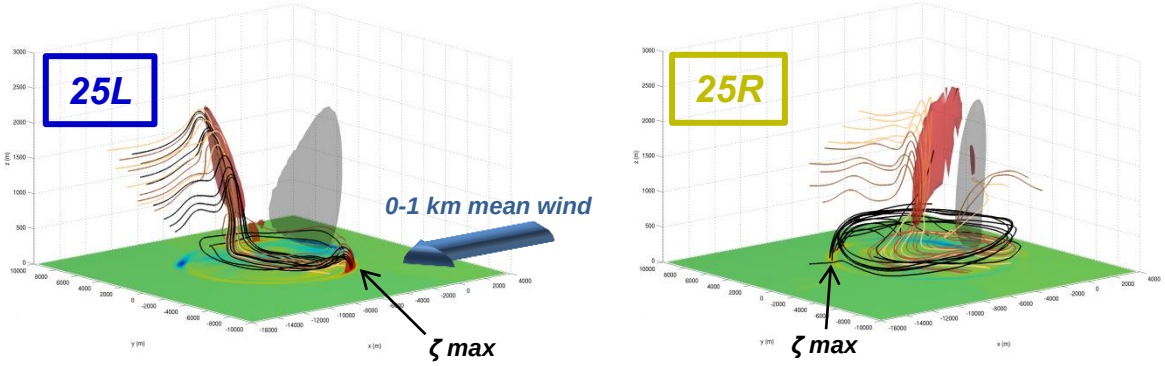

Figure 4: Same as Figure 2 except for the 25L (left) and 25R (right) hodographs using the cooling tendency forcing. In this case, vortex lines are drawn through the 20 highest vertical vorticity pixels at 0, 500, and 1000 m AGL. The orientation of the 0-1 km mean wind vector is shown schematically for reference.

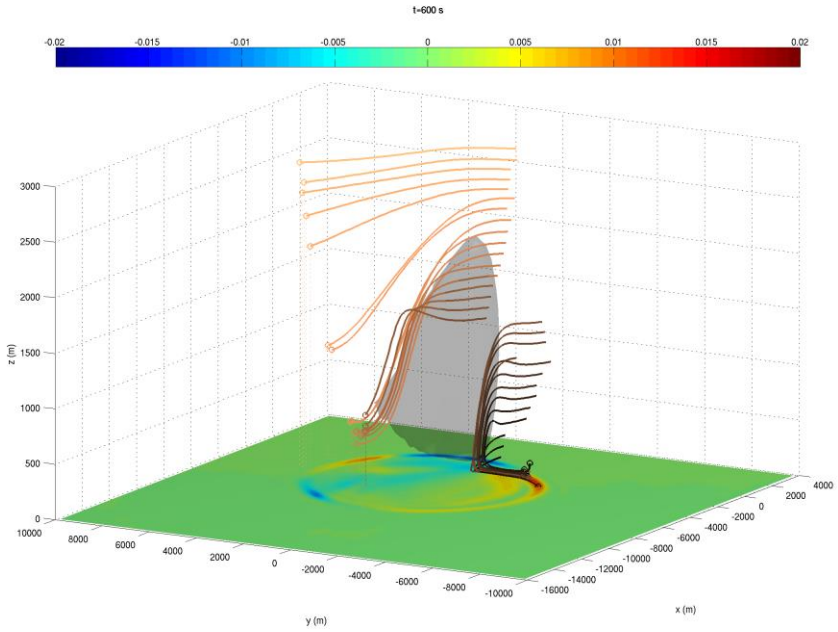

Figure 5: Three-dimensional projection of parcel trajectories, surface vertical vorticity (shaded as shown), and isosurface of vertical velocity (gray, as in Figure 2) for the simulation using the 25L hodograph with cooling tendency forcing. The trajectories shown are for the parcel initially from each model level that ultimately has the largest vertical vorticity value during the simulation. The trajectories' ending points at t=10 min are plotted as circles.